New environment for a two-dimensional topological insulator with hexagonal channels hosting diiodido-bismuthate(I) anions in singlet state

Supporting Information

Bertold Rasche [1], Wouter Van den Broek [3] and Michael Ruck [1, 2*]

1 Department of Chemistry and Food Chemistry, TU Dresden, 01062 Dresden, Germany

2 Max Planck Institute for Chemical Physics of Solids, 01187 Dresden, Germany

3 Institute of Experimental Physics, University of Ulm, 89069 Ulm, Germany

Table S1: Extrapolated principal mean square displacements (/10^{-1} pm^2) at 0 K together with the mean value and the standard deviation for all atoms in $Bi_{38}Pt_9I_{14}$. Bi4, I1, I2 and I5 are residing in the hexagonal the channels.

atom	principal mean square displacement at 0K			mean value	standard deviation
Pt1	2.7	1.9	2.2	2.3	0.4
Pt2	2.2	2.1	2.4	2.3	0.1
Bi1	2.9	2.5	2.2	2.5	0.3
Bi2	4.2	2.5	2.7	3.1	0.9
Bi3	3.5	2.3	1.9	2.6	0.9
Bi4	4.9	3.5	3.5	4.0	0.8
I1	4.0	5.0	5.0	4.7	0.6
I2	6.5	2.2	2.2	3.6	2.5
I3	6.7	4.5	2.6	4.6	2.0
I4	5.5	4.4	3.4	4.4	1.1
I5	7.1	7.1	6.4	6.8	0.4

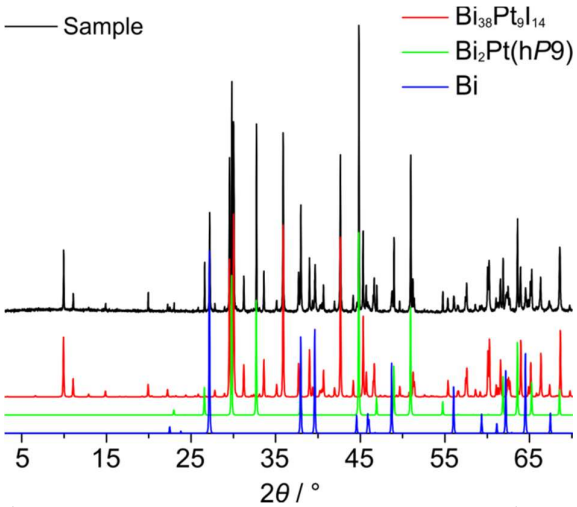

Figure S1: PXRD data of a sample (Bi, BiI_3 and Pt in the molar ratio Bi:Pt:I = 38:9:14) annealed for one week at 290 °C; and reference PXRD-patterns of $Bi_{38}Pt_9I_{14}$, Bi and Bi_2Pt(*hP*9).

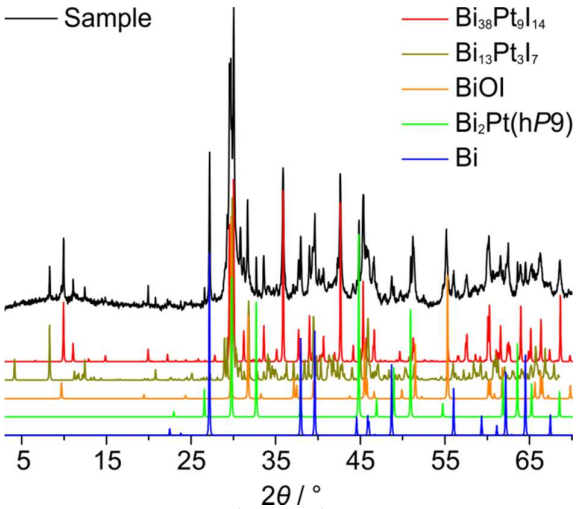

Figure S2: PXRD data of a sample after a DSC-experiment (Figure 2) with reference PXRD-pattern of $Bi_{38}Pt_9I_{14}$, $Bi_{13}Pt_3I_7$, BiOI, Bi and Bi_2Pt(*hP*9). Most probably, BiOI was formed by reaction of BiI_3 with moisture from air during the preparation of the PXRD sample.

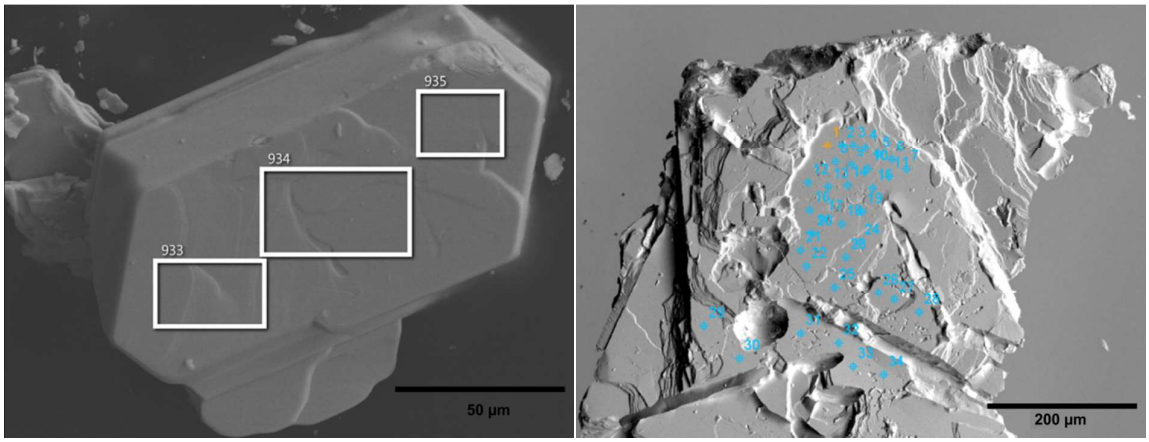

	Bi / at%	Pt / at%	I / at%
Experimental Data			
Figure S3(a)	64.7(8)	14.6(1)	20.6(8)
Figure S3(b)	64(1)	15(1)	21(1)
Calculated Compositions			
$Bi_{38}Pt_9I_{14}$	62.3	14.8	23.0
$Bi_{36}Pt_{11}I_{14}$	59.0	18.0	23.0
$Bi_{36}Pt_9I_{16}$	59.0	14.8	26.2

Figure S3 and Table S2: Scanning microscopy pictures of two different $Bi_{38}Pt_9I_{14}$ crystals with marked areas/spots were EDX spectra were taken. The quantitative results are summarized in Table S2 and compared to possible theoretical compositions.

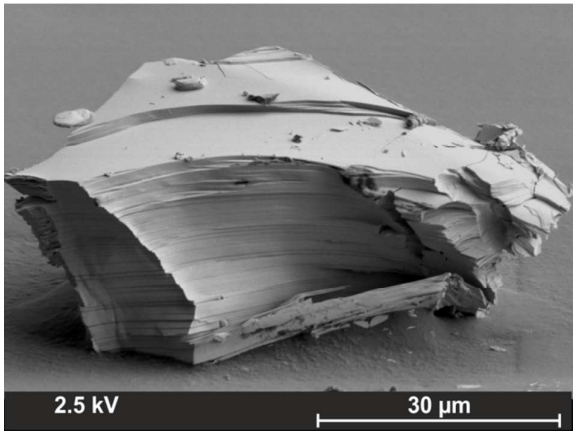

Figure S4: Scanning electron microscopy picture of a tilted $Bi_{38}Pt_9I_{14}$ crystal.

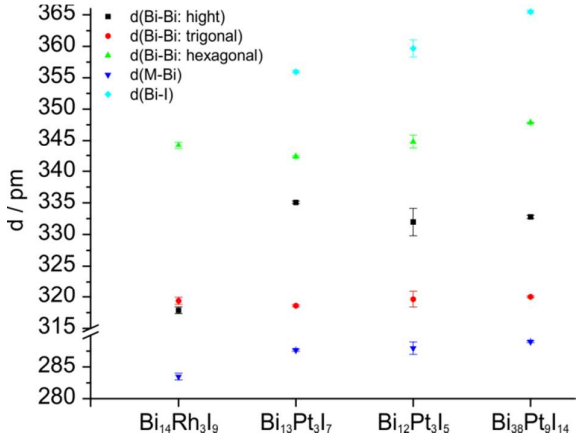

Figure S5: Distances of bismuth atoms in the intermetallic layer to the three types of surrounding bismuth atoms (black, red, green), to the transition element (blue) and to the iodide ions of the separating iodide layer (cyan) for the all known compounds with the intermetallic layer as structural fragment. The given error bars indicate +/−3σ calculated from the e.s.d.s of the atomic positions.

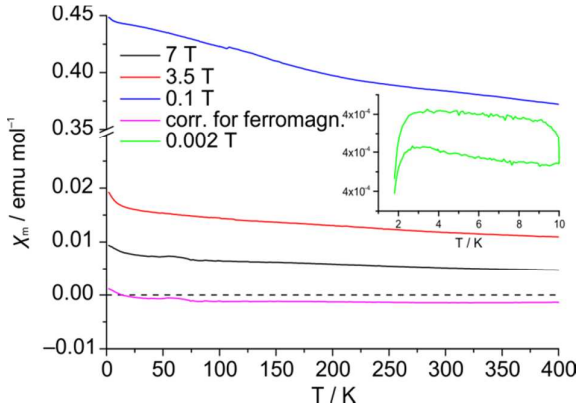

Figure S6: Magnetic susceptibility vs. temperature of $Bi_{38}Pt_9I_{14}$ in different magnetic fields. The inset shows the behaviour in very low fields to check for superconductivity down to 2 K.

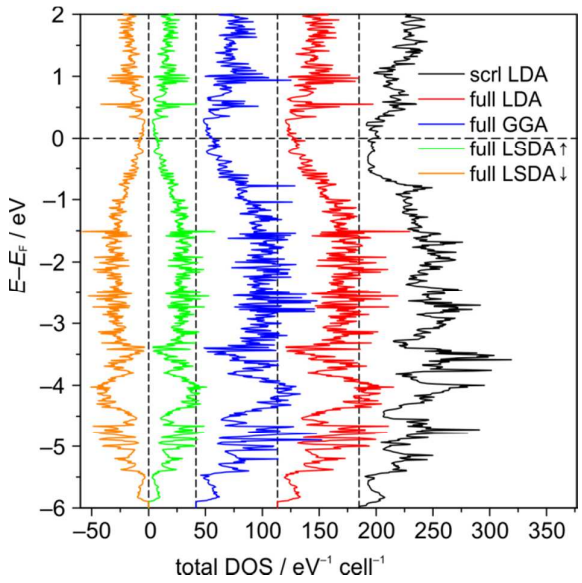

Figure S7: Total density of states (DOS) for $Bi_{38}Pt_9I_{14}$ from scalar-relativistic (scrl) and full-relativistic (full) DFT calculations, with different exchange correlation potentials (local density approximation: LDA; generalised gradient approximation: GGA; local spin density approximation: LSDA). Vertical dashed lines mark the respective zero value.

Table S3: Strong and weak topological invariants, as well as the δ_i values calculated from the parity eigenvalues at the time-reversal invariant momenta (TRIM) for bands close to the Fermi level. The latter is indicated by the fat line.

band energy at Γ /eV	occupation	topological invariants		δ_i values at all eight TRIM							
				Γ	M		K	A	L		H
		strong	weak	[000]	[100]	[010]	[110]	[001]	[101]	[011]	[111]
−0.55477	full	1	(001)	1	1	1	1	1	−1	−1	−1
−0.41229	full	1	(000)	−1	1	1	1	−1	−1	−1	−1
−0.26756	partial	0	(001)	1	−1	−1	−1	−1	1	1	1
−0.05624	partial	1	(000)	1	−1	−1	−1	1	1	1	1
0.05404	partial	1	(000)	−1	1	1	1	1	1	1	1
0.08552	empty	1	(000)	−1	1	1	1	−1	−1	−1	−1
0.26862	empty	1	(000)	−1	1	1	1	−1	−1	−1	−1